CDC50 orthologues in *Plasmodium falciparum* have distinct roles in merozoite egress and trophozoite maturation

Avnish Patel[1], Stephanie D. Nofal[1], Michael J. Blackman[2] and David A. Baker[1]

1. Department of Infection Biology, London School of Hygiene & Tropical Medicine, London, United Kingdom

2. Malaria Biochemistry Laboratory, The Francis Crick Institute, London, United Kingdom and Department of Infection Biology, London School of Hygiene & Tropical Medicine, London, United Kingdom.

Abstract

In model organisms P4-ATPases require cell division control protein 50 (CDC50) chaperones for their phospholipid flipping activity. In the malaria parasite, *P. falciparum,* guanylyl cyclase alpha (GCα) is an integral membrane protein that is essential for release (egress) of merozoites from their host erythrocytes. GCα is unusual in that it contains both a C-terminal cyclase domain and an N-terminal P4-ATPase domain of unknown function. We sought to investigate whether any of the three CDC50 orthologues (denoted A, B and C) encoded by *P. falciparum* are required for GCα function. Using gene tagging and conditional gene disruption, we demonstrate that both

CDC50B and CDC50C are expressed in the clinically important asexual blood stages and that CDC50B is a binding partner of GCα whereas CDC50C is the binding partner of another putative P4-ATPase, ATP2. Our findings indicate that CDC50B has no essential role for intraerythrocytic parasite maturation but modulates the rate of parasite egress by interacting with GCα for optimal cGMP synthesis. In contrast, CDC50C is essential for blood stage trophozoite maturation. Additionally, we find that the CDC50C-ATP2 complex may influence parasite endocytosis of host cell haemoglobin and consequently hemozoin formation.

Introduction

Plasmodium falciparum is responsible for the majority of malaria mortality and morbidity globally. Whilst there was a sharp reduction in malaria-related deaths between 2000 and 2014 due to increased surveillance, improved control measures and the use of highly effective drug treatments, the decline in cases has halted in recent years. This is thought to be due to the emergence of resistance to insecticides in the *Anopheles* mosquito vector, and to the appearance of parasites resistant to artemisinin combination therapies (ACTs) (1). Given this trend, novel targets must be explored to generate candidates for the drug development pipeline to prevent a future increase in disease burden should the ACTs fail (2).

P. falciparum has a complex life cycle, characterised by multiple specialised developmental forms which transition between the mosquito vector and humans (3). Malaria pathology is caused exclusively by the asexual blood stage of the life cycle. Briefly, extracellular merozoites

invade host erythrocytes and transform into ring stages for around 24 h. These develop within a membrane-enclosed parasitophorous vacuole to form trophozoites which digest host cell haemoglobin and initiate DNA replication and endomitosis. The resulting schizonts undergo cytokinesis (segmentation) only upon maturation, forming daughter merozoites which are released from the host cell through a highly regulated egress process. The cycle is then re-initiated by the invasion of fresh erythrocytes by the newly released merozoites. A detailed molecular understanding of the biochemical pathways and proteins essential for blood-stage development will inform discovery of novel targeted therapeutics that prevent malaria pathogenesis.

Merozoite egress and invasion are regulated by cyclic nucleotide signalling, conserved elements of which regulate multiple aspects of cell biology in model organisms and across the animal kingdom and can be effectively targeted pharmacologically (4). The second messengers cyclic adenosine monophosphate (cAMP) and cyclic guanosine monophosphate (cGMP), are produced by cyclase enzymes and activate their respective cyclic nucleotide-dependent effector protein kinases PKA and PKG in a concentration-dependent manner (5). The activated kinases phosphorylate downstream targets which carry out effector functions and the cyclic nucleotide signals are then broken down by phosphodiesterases (6, 7). *P. falciparum* uses cyclic nucleotide signalling throughout its complex life cycle (7). Notably, cGMP signalling is required for egress of asexual blood stage merozoites (8, 9) but also egress of gametes (10) and liver stage parasites (11, 12) as well as for ookinete and sporozoite motility (12–14). In contrast, cAMP signalling has been shown to be required for sporozoite apical organelle secretion and invasion of hepatocytes (15), gametocyte deformability (16) and erythrocyte invasion (17).

P. falciparum has two guanylyl cyclases. Whilst guanylyl cyclase beta (GCβ) is dispensable in blood stages (9), guanylyl cyclase alpha (GCα) synthesises cGMP in mature blood stage schizonts, where it plays an essential role in activating PKG to trigger egress (18). Both of the malaria parasite GCs are large integral membrane proteins with 22 predicted transmembrane domains (TMDs), the C-terminal segment of which constitutes the paired C1 and C2 guanylyl cyclase catalytic domains. Uniquely for cyclase enzymes, *Plasmodium* GCs (along with apicomplexan and ciliate orthologues) also contain an N-terminal Type IV P-type ATPase (P4-ATPase)-like domain (18–20). In other organisms P4-ATPases transport phospholipids from the outer to the inner leaflet of a lipid bilayer, maintaining lipid asymmetry required for numerous functions including membrane remodeling and vesicle formation (21). Recent studies in the apicomplexan parasite *Toxoplasma* indicate that this domain is critical to the role of its single guanylyl cyclase TgGC in lytic growth, where it is essential for host cell attachment, invasion and motility-dependent egress of tachyzoites (22–25).

In model organisms, P4-ATPases require cell division control protein 50 (CDC50) chaperones for their phospholipid flipping activity (26, 27). CDC50 proteins are integral membrane proteins with two TMDs (28, 29). Studies in yeast have shown that CDC50 binding partners are required for the auto-phosphorylation of the catalytically active aspartic acid residue of the P4-ATPase, which is necessary for completion of the phospholipid flipping reaction cycle (30, 31). *P. falciparum* encodes three putative CDC50 proteins, termed CDC50A (PF3D7_0719500), CDC50B (PF3D7_1133300) and CDC50C (PF3D7_1029400). Previous work in the mouse malaria model *P. yoelii* has shown that CDC50A binds to GCβ and is required for ookinete motility (20). Similarly, TgGC controls egress of tachyzoites (22, 24, 25) and binds to a *Toxoplasma* CDC50 partner

which is required for its function (22). However, the functions of *P. falciparum* CDC50 orthologues have not been examined. Here we show that both CDC50B and CDC50C are expressed in the asexual blood stages and that CDC50B interacts with GCα whereas CDC50C is the binding partner of another putative P4-ATPase (ATPase2; PF3D7_1219600). We show that CDC50B modulates the efficiency of parasite egress by interacting with GCα for optimal cGMP synthesis. In contrast, CDC50C is essential for asexual blood stage trophozoite maturation due to a crucial role in endocytosis of host erythrocyte haemoglobin.

Results

1) Generation of genetic tools to investigate the function of the *P. falciparum* CDC50s

To assess the biological functions of CDC50A, B and C in *P. falciparum* blood stages, we generated three transgenic parasite lines designed to allow investigation of subcellular location and the effects of conditional disruption of each CDC50. The transgenics were generated in the genetic background of a 3D7 *P. falciparum* line that stably expresses dimerisable Cre (DiCre), the Cre-recombinase activity of which is induced in the presence of rapamycin (RAP) (32, 33). In each case, the target genes were 'floxed' such that treatment with RAP would lead to excision of DNA sequences encoding a C-terminal region containing the second TMD of each protein (Fig 1 A and B); this TMD has been shown in model organism CDC50-ATPase structures to interact with the C-terminal helix of the ATPase binding partner (28, 29). The constructs were designed

so that following homologous recombination, the genes were also modified by fusion to sequences encoding a C-terminal triple hemagglutinin (HA) epitope tag.

Successful modification of the target genes was verified by PCR (Fig 1C), and expression and RAP-induced excision of tagged CDC50A-HA, CDC50B-HA and CDC50C-HA fragments in the respective transgenic parasites (termed CDC50A-HA:loxP, CDC50C-HA:loxP and CDC50B-HA:loxP) was confirmed by western blot (Fig 1D). Immunofluorescence analysis (IFA) of the transgenic lines (Fig 1E) revealed a diffuse, partly peripheral signal in individual merozoites within mature segmented schizonts for both CDC50B-HA and CDC50C-HA. This was similar to the pattern observed upon co-staining with the plasma membrane marker, merozoite surface protein 1 (MSP1). Whilst successful tagging and floxing of the *CDC50A* gene was also confirmed by PCR and Sanger sequencing, no protein expression could be detected in asexual blood stages. This suggested that CDC50A is not expressed in asexual stages, consistent with findings in *P. yoelii* where it is expressed only in gametocyte and mosquito stages (20). Alternatively, since *P. falciparum* transcriptomic data indicates that the *CDC50A* gene is transcribed in schizont stages (34), the protein may be expressed but rapidly degraded as its GCβ binding partner is not present in asexual blood stages (9, 19).

2) Of the three isoforms, only CDC50C is essential for blood stage parasite growth

To investigate the essentiality of CDC50A, CDC50B and CDC50C, highly synchronised ring-stage cultures of each DiCre transgenic line were treated with RAP to induce excision of the sequence encoding the C-terminal TMD of each protein (Fig 1C), and parasite replication assessed using

flow cytometry (Fig 3A). RAP-treated CDC50A-HA:loxP and CDC50B-HA:loxP parasites displayed no significant growth inhibition over three cycles compared to matched control (DMSO-treated) parasites (Fig 2A). In contrast, CDC50C-HA:loxP parasites underwent complete growth arrest after cycle 1. Examination of the parasites by Giemsa-staining showed that whilst new rings went on to form schizonts in DMSO-treated WT parasites, RAP-treated CDC50C-HA:loxP rings did not develop beyond the early trophozoite stage and eventually collapsed into small vacuoles (Fig 2B). It was concluded that CDC50C is essential for asexual blood stage survival.

3) CDC50B and CDC50C bind to distinct parasite flippase partners

In other organisms, CDC50 proteins interact with their cognate P4-ATPases and are required for their activity (28–31). To determine whether CDC50B and CDC50C interact with P4-ATPases in *P. falciparum* blood stage development we performed immuno-precipitation (IP) experiments from extracts of highly synchronised CDC50B-HA:loxP and CDC50C-HA:loxP schizonts. Western blot analysis confirmed the expected enrichment of the HA-tagged proteins from schizont lysates (Fig 3A). The immuno-precipitated material was then analysed by mass spectrometry in comparison with mock IP samples to confirm this and identify co-precipitating protein species. This confirmed high levels of enrichment of the HA-tagged CDC50 bait proteins (Fig 3B). In addition, in the case of the CDC50B experiments we detected a >9 $\log_2$ enrichment of peptides derived from GCα (Fig 3B), whilst in the CDC50C IPs we detected >9 $\log_2$ enrichment of peptides mapping to another putative P4-ATPase, a putative amino-phospholipid flippase PF3D7_1219600 (ATP2) (Fig3B). No other proteins were as significantly enriched in each pull-

down. These results strongly suggest that CDC50B is a co-factor for GCα and CDC50C is a co-factor for ATP2.

4) CDC50B is not required for GCα expression or trafficking, but is crucial for optimal cGMP synthesis required for egress

GCα has a key role in egress, as the source of cGMP required for PKG activation (18). Having determined that CDC50B interacts with GCα, we next investigated whether CDC50B also has a role in parasite egress.

To do this, we first compared the egress kinetics of mature DMSO- and RAP-treated CDC50B-HA:loxP schizonts by monitoring the appearance in culture supernatants over time of proteolytically processed forms of the PV protein serine repeat antigen 5 (SERA5), as a proxy for egress (35). As shown in Fig 4A, this revealed a marked reduction in the rate of egress over the sampling period in RAP-treated CDC50B-HA:loxP parasites as compared to control DMSO-treated counterparts. Densitometric quantitation of data from three independent biological replicate experiments indicated that CDC50B null schizonts undergo ~50% less egress than WT controls when sampled over two hours (Fig S1). This was not due to a delay in schizont development, since Giemsa staining of DMSO- and RAP-treated CDC50B schizonts showed no detectable delay in parasite maturation, and analysis of DNA content by flow cytometry indicated no significant differences between formation of DMSO- and RAP-treated CDC50B schizonts (Fig 4A lower).

In *T. gondii*, the orthologue of CDC50B is required for correct subcellular trafficking of TgGC (22). To investigate whether this is also true in *P. falciparum*, we used a CRISPR-Cas9-based approach to fuse GCα to a C-terminal mCherry tag in the CDC50B-HA:loxP line, creating a parasite line called CDC50B-HA:loxP GCα-mCherry (Fig S2). We failed to detect the tagged protein directly by fluorescence microscopy, possibly due to the previously reported very low abundance of GCα (18). However, western blot revealed a ~250 kDa signal in schizont lysates from CDC50B-HA:loxP GCα-mCherry schizonts, likely representing a proteolytic fragment of the tagged protein, since GCα is prone to proteolytic degradation in both *P. falciparum* and *T. gondi* (18, 22) (Fig 4B). Interestingly, western blot of extracts of RAP-treated CDC50B-HA:loxP GCα-mCherry schizonts indicated that there was no marked reduction in the levels of GCα in the absence of CDC50B (Fig 4B). Exploiting the tagged GCα-mCherry line, we sought to confirm whether CDC50B was co-precipitated when GCα-mCherry was immuno-precipitated using RFP-trap beads. Co-precipitation of CDC50B was observed, confirming CDC50B binding by GCα-mCherry (Fig 4C).

To examine the role of CDC50B in trafficking of GCα, we used an anti-mCherry antibody to localize GCα-mCherry by IFA in RAP-treated CDC50B-HA:loxP GCα-mCherry parasites. This revealed no obvious mis-localisation of GCα in the absence of CDC50B, with a similar, diffuse signal detectable in both RAP- and DMSO-treated schizonts. In addition, in contrast with *T. gondii* (20), no mislocalisation of GCα in the ER or secretory pathway in the absence of CDC50B was detected, as judged by co-localisation with the ER marker plasmepsin V (PMV) (Fig 4E). Taken together, these results indicate that CDC50B binding is not important for the correct trafficking or stable expression of GCα. To seek more insight into the egress defect, we

investigated whether ablation of CDC50B resulted in changes in cyclic nucleotide levels. To do this, we assayed extracts of DMSO- and RAP-treated CDC50B-HA:loxP schizonts by ELISA to quantitate cGMP and cAMP levels. This showed that CDC50B null parasites contained 53.67% (±12.16%) less cGMP than DMSO-treated controls, whilst no significant difference in cAMP levels was observed (Fig 4F). These reduced cGMP levels suggested that binding of CDC50B to GCα might be required for maximal GCα cyclase activity. To test this, we investigated whether the defect in egress of CDC50B null schizonts could be reversed by the addition of compounds that stimulate or mimic elevated cGMP levels. Egress was monitored in the presence and absence of the PDE inhibitor zaprinast or PET-cGMP, a membrane-permeable cGMP analogue known to activate parasite PKG (18, 36). Treatment with either compound restored egress of CDC50B null schizonts to levels similar to those observed in control CDC50B-HA:loxP schizonts, confirming the requirement of CDC50B for optimal cGMP synthesis by GCα (Fig 4G).

In view of the above results, as well as the previous observation that a lipid co-factor may stimulate egress in *Toxoplasma* and *P. falciparum* (22, 37), we examined whether the potential phospholipid flippase activity of the P4-ATPase domain of GCα might be modulated by CDC50B binding. To do this, we investigated whether uptake of fluorescently-labelled PS, PE and PC were affected following excision of CDC50B. DMSO- or RAP-treated CDC50B-HA:loxP late schizonts were incubated with fluorescent lipids, then analysed by flow-cytometry to determine their ability to accumulate lipids. We found no significant difference in the bulk uptake of measured lipids in schizonts in the presence or absence of CDC50B (Fig S3).

5) CDC50C is not required for lipid uptake or protein export, but plays an essential role in haemoglobin uptake from the host erythrocyte.

As described above, RAP treatment of synchronous, newly invaded CDC50C-HA:loxP rings produced a CDC50C null parasite population that displayed a trophozoite arrest phenotype (Fig 2B), suggesting an essential role for CDC50C in the trophozoite-to-schizont transition. Given this evidence that CDC50C plays a very different role to that of CDC50B, we decided to interrogate more precisely the functional role of CDC50C. Previous transcriptomic analysis has shown that CDC50C is transcribed throughout the asexual blood stage cycle, with relatively low levels of transcription in rings increasing to a peak in mature schizont stages (34). Consistent with this transcriptional profile, immuno-staining of CDC50C-HA:loxP parasites detected expression in ring, trophozoite and schizont stages (Fig S4). Co-staining of CDC50C in trophozoites with antibodies to ERD2 (a Golgi marker), PMV (an ER marker) or EXP2 (a PVM marker) showed that CDC50C displayed a diffuse cytosolic staining with no clear subcellular localisation (Fig5A).

Phospholipid flippases have been shown to contribute directly to cellular lipid uptake (38–40). Initially we speculated that the growth arrest of CDC50C null trophozoites may be due to a dysregulation of lipid uptake as a result of loss of function of the putative amino-phospholipid flippase ATP2 partner. To test this notion, we labelled live RAP- and DMSO-treated CDC50C-HA:loxP trophozoites with the fluorescent amino-phospholipid analogues NBD-PC, NBD-PE and NBD-PS. No discernable difference in lipid uptake between CDC50C null and WT trophozoites was observed by microscopy (Fig 5B), suggesting that CDC50C plays no essential role in uptake of these phospholipids.

In model organisms, flippases also contribute to the production and maintenance of membrane asymmetry required for generation of trafficking vesicles, with specific flippases influencing exocytosis or endocytosis pathways (41–44). Given that lipid uptake was unaffected in the absence of CDC50C, we considered it plausible that the ATP2-CDC50C complex may contribute to lipid homeostasis and trafficking in an analogous manner. *P. falciparum* trophozoites re-model their intracellular environment to create new permeation pathways that enable export of a wide variety of proteins into the host RBC via exocytosis, a process which is essential for trophozoite development (45). To examine whether trophozoite death in CDC50C null parasites could be attributed to changes in protein exocytosis, control or RAP-treated CDC50C-HA:loxP ring stage parasites were allowed to develop into trophozoites then analysed by IFA to determine the localisation of skeleton binding protein (SBP), a prominent exported protein in trophozoites. Puncta of SBP, characteristic of export, were evident within the RBC cytosol in both DMSO- and RAP-treated CDC50C-HA:loxP trophozoites (Fig 6A), and quantification of these puncta indicated that there was no significant change in the levels of export of SBP in CDC50C null trophozoites (Fig 6B). This suggested that loss of CDC50C has no impact on bulk protein export during trophozoite development.

As protein export and possibly exocytosis of CDC50C null trophozoites was unaffected we lastly examined an essential endocytotic process. As intracellular asexual blood stage malaria parasites develop, they endocytose and digest host erythrocyte haemoglobin. A major by-product of this catabolic process is the sequestration of haem in the form of a characteristic crystalline product called haemozoin, which accumulates in the parasite digestive vacuole as large, refractile complexes that are easily visible by light microscopy. Microscopic examination

of Giemsa-stained thin blood films indicated that whilst CDC50C null trophozoites displayed an apparently normal morphology, the hemozoin crystals appeared smaller than those of DMSO-treated controls (Fig 6C right). To examine this in greater detail, we compared the ratio of the hemozoin crystal length to that of the parasite length in RAP- and DMSO-treated CDC50C null trophozoites. This confirmed a significantly decreased ratio in CDC50C null trophozoites (Fig 6C), suggesting a CDC50C-dependent defect in haemozoin formation. To further examine this, we purified and quantified haemozoin from parallel populations of RAP- and DMSO-treated CDC50C-HA:loxP trophozoites (46). As shown in Fig 6D, this revealed ~30% less hemozoin in trophozoites lacking CDC50C. To investigate whether uptake of haemoglobin was affected in CDC50C null trophozoites, RAP- and DMSO-treated CDC50C-HA:loxP trophozoites were harvested at 36 h post invasion, released from their host cells using saponin, and levels of intra-parasite haemoglobin quantified by western blotting (Fig 6E). The results indicated that the levels of haemoglobin within CDC50C null trophozoites was significantly reduced compared with control counterparts (Fig S5). Collectively, these data support a role for CDC50C in uptake and digestion of host erythrocyte haemoglobin that is essential for parasite development.

Discussion

In this study we have shown that CDC50B and CDCD50C proteins are expressed during asexual blood stage development, and that they each bind to different putative P4-ATPase flippases - GCα and ATP2 respectively - which function at different developmental stages of the asexual blood stage cycle. CDC50B is dispensable for intraerythrocytic development, as is its orthologue

in *P. yoelii* (20). However, we find that cGMP levels are reduced in CDC50B null parasites as well as rates of egress. This defect can be rescued by treatment of CDC50B null parasites with either the PDE inhibitor zaprinast or PET-cGMP, membrane-permeable cGMP analogue known to be capable of activating apicomplexan PKGs (18). As no growth defect was observed in CDC50B null parasites, it seems that whilst egress rates are reduced, CDC50B parasites are egress competent and do eventually egress. Collectively, our results strongly suggest that CDC50B acts to enhance cGMP synthesis by GCα. Recent studies in *T. gondii* have shown that the single GC (TgGC) also binds to a CDC50 designated CDC50.1 (22). In contrast to the present study, knockdown of CDC50.1 resulted in mis-localisation of TgGC and a block in egress of *T. gondii* tachyzoites (22). The egress block could be rescued by adding a PDE inhibitor, implying that in the absence of CDC50.1, TgGC remains functional but produces cGMP with reduced efficiency (20). We observed no detectable mislocalisation of *P. falciparum* GCα in the absence of CDC50B, with normal growth of parasites albeit with reduced egress rates, indicating differences between the genera. We speculate that this may be due to differences in the threshold levels of cGMP required to activate PKG to trigger egress in each species.

Importantly, our work adds to the evidence supporting a role for CDC50s and the P4-ATPase domain of apicomplexan GCs acting functionally to stimulate maximal cGMP production required for egress. By analogy with other CDC50-flippase interactions, we can deduce that this occurs through CDC50B binding to the P4-ATPase domain of GCα. Modulation of the activity of the C-terminal cyclase domain by the P4-ATPase may integrate a lipid-mediated trigger for egress, potentially by phosphatidic acid as shown in *T. gondii* (22) or phosphatidylcholine (PC) as recently indicated in *P. falciparum* (37). However, we did not observe changes in the bulk

uptake of fluorescent PC by schizonts lacking CDC50B. Recent structural examination of a human P4-ATPase:CDC50 complex has shown that CDC50 forms an intimate interaction with the TMDs of the P4-ATPase partner, with the loop domain between the two TMDs of the CDC50 forming an anti-parallel beta-sheet structure that contacts the luminal side of the transmembrane loops of the P4-ATPase. Human CDC50 is glycosylated at several conserved asparagine residues, and the structure showed that interactions between CDC50 glycan moieties and P4-ATPase stabilise the functional complex (29). Intriguingly an alignment of human CDC50a and the three *P. falciparum* CDC50s indicates that Asn180, at which glycosylation has been shown to interact structurally with its partner P4-ATPase (29), is absent from CDC50B but conserved in both CDC50A and C (Fig S6). N-glycosylation has been observed in *P. falciparum* (47), but this finding raises the possibility that CDC50B may be non-glycosylated. This observation may explain the finding in *P. yoelii* that GCβ is degraded in the absence of its partner CDC50, suggesting that GCβ is highly reliant on interactions with its CDC50 partner (CDC50A) for protein stabilization (20). In contrast, in our study we observe that loss of CDC50B does not impact on expression of GCα, since GCα-mediated egress still occurs.

The revelation that CDC50C is essential for intraerythrocytic maturation of asexual blood stage *P. falciparum* trophozoites and that CDC50C binds to ATP2 suggests that CDC50C plays a role critical for ATP2 function. In contrast to our findings using native parasite-derived protein preparations, a recent *in-vitro* study using recombinant protein indicated that ATP2 can bind CDC50B; however, CDC50C binding was not tested in that work as the authors could not express it (48). Our study indicates that the essential function of CDC50C cannot be complemented by CDC50B.

315 Global transposon mutagenesis data suggest that the gene encoding ATP2 is essential in *P.*
316 *falciparum* blood stages (49) and its orthologue is refractory to targeted deletion in *P. berghei*
317 (50). Whilst its cellular function is unknown, ATP2 has been implicated in resistance to two
318 Medicines for Malaria Venture (MMV) 'Malaria box' compounds, mediated through a novel
319 pathway involving gene copy number amplification. Functional characterisation of the
320 mechanism by which drug resistance is achieved remains lacking (51). Interestingly, Cowell et
321 al. observed non-synonymous mutations in genes encoding putative parasite Sec24 and Yip1
322 proteins (classically involved in vesicular trafficking) in drug resistant parasite lines containing
323 *ATP2* copy number variations (51). Here we found that the ATP2-CDC50C complex influences
324 endocytosis of haemoglobin during blood stage development possibly by influencing the
325 phospholipid makeup of the cytostome, a structure that is crucial for hemoglobin uptake (52,
326 53), and it remains possible that other endocytic pathways may also be affected by loss of ATP2
327 function, although these were not investigated. In yeast, different P4-ATPases contribute to
328 distinct vesicular trafficking pathways (43, 44). It is plausible that this could be similar in *P.*
329 *falciparum*. We speculate that copy number modulation of *ATP2* acquired during selection for
330 drug resistance may modulate the endocytic pathway of the parasite so as to affect drug
331 uptake, although further work is required to investigate this.

332 A recent study in *P. yoelii* has shown that the orthologue of CDC50C binds to a different P4-
333 ATPase (ATP7) in ookinetes during parasite development within the mosquito (54). This
334 indicates that CDC50C chaperones the activity of distinct P4-ATPases in different developmental
335 stages of the parasite life cycle, in both mammalian and insect hosts. Consistent with this, the
336 transcriptomic profiles of *ATP2* and *ATP7* show that they are confined to asexual and insect
337 stages respectively. The same study demonstrated that the ATP7-CDC50C complex is required

for PC uptake in ookinetes and the authors suggested that this process may be required to allow mosquito midgut cell traversal, as CDC50C null or ATP7 null ookinetes could not achieve this. Intriguingly, alignment of ATP7 and ATP2 primary sequences alongside those of model P4-ATPases revealed that the 'QQ motif' involved in defining substrate specificity is replaced by QL and QV respectively (Fig S7). Given the similarity between these amino acid motifs, it is plausible that ATP2 also transports PC. Our finding that NDB-PC uptake is unaffected in CDC50C null trophozoites suggests that either ATP2 transports another phospholipid or that lipid uptake in trophozoites occurs via (multiple) redundant pathways. During the preparation of this manuscript, a recent pre-print has found that the *T. gondii* orthologue of CDC50C, CDC50.4, binds ATP2B an essential P4-ATPase that transports PS (55). This CDC50.4-ATP2B complex is required for efficient mirconeme secretion of tachyzoites with no defect observed during parasite intracellular development (55). It is plausible the *P. falciparum* CDC50C-ATP2 complex may perform a similar role in egressed merozoites, however, this was not addressed in our study due to the block of intra-erythrocyte development in CDC50C null parasites. Our work provides substantial new insights into the multifaceted, essential roles played by CDC50C proteins in malaria parasites and highlights potential species-specific divergences in the role of CDC50s in Apicomplexa.

Materials and methods

P. falciparum culture and synchronisation

P. falciparum erythrocytic stages were cultured in human erythrocytes (National Blood Transfusion Service, UK) and RPMI 1640 medium (Life Technologies) supplemented with 0.5% Albumax type II (Gibco), 50 µM hypoxanthine, and 2 mM L-glutamine. Synchronous parasite cultures were obtained as described previously (56). Briefly, late segmented schizonts were enriched by centrifugation on a 60% Percoll (GE Healthcare) cushion, followed by the addition

of fresh erythrocytes to allow invasion for 1–2 h under continuously shaking conditions. Remaining schizonts were then removed by sorbitol treatment to yield highly synchronous ring-stage cultures. In all cases, induction of DiCre activity when required was by treatment for 2–4 h with 100 nM RAP (Sigma) as described previously (32, 57). Control parasites were treated with vehicle only (1% v/v DMSO).

Genetic modification of *P. falciparum* parasites

The CDC50A-HA:loxP, CDC50B-HA:loxP and CDC50C-HA:loxP lines were generated from the DiCre-expressing 3D7 (33) *P. falciparum* clone using SLI of a plasmid containing a SERA2loxPint (57) followed by a triple-HA tag and an in frame Thosea asigna virus 2A (T2A) ribosomal skip peptide and NeoR cassette with a downstream loxP and PbDT 3'UTR sequences as described previously. Re-codonised versions of the C-terminal portion of each gene containing the last transmembrane helix were synthesised commercially (IDT) and inserted downstream of the SERA2loxPint and upstream of the 3×HA tag. Sequences as follows: CDC50A – GATTTCTGGCTCATGAACGAAAAGTACAAGAACGCATTAAACATGAACAATGAGAACGGTTACGGTGAC GAAAACAGTCACTTCATAGTTTGGATGAAGACTGCAGCTTTGAGTGAATTTAGAAAGAAGTACGCAAAG ATTAACGTAGAGGTAAACTTGCCTATTTACGTTAACATAAACAACAACTTCCCAGTCACCAAGTTCAACG GAAAGAAGTTCTTCGTAATCGCAGAGGGTAGTATTTTCATTAACGAGAAGATTCAGTCTCTCGGTATTCT CTATTTGGTTATAGGTATAATTAGTCTAGGTATAGTTGCATGCCTTATTTACAACCAGATGAAGAATCCG AGGATAATTGGATATCACGCTTATATTTACATCTTCTTCTTCTTGG; CDC50B – GATCACATTTACTTTTGGATGGAGCCTGATATTCAGTACGAGCGTTTGCAGGAGAACAAGGAGACTAAC

GAGAAATTGCTAGTTTTGCCTCAGACTTTGAAGTACAACCAGGCTGGTAAGGCAATTGAGAATTCTCACT
TCATAAACTGGATGATTCCTAGTGCTCTAAACTACATAAAGCGATTGTACGGAAAGTTGTACATTCCATT
GAAGTTCCCCTTCTACATCTACATTGAGAACAACTTCAAGATAAACGACACTAAGATAATCGTAATATCT
ACATCTCAGTACTACATGAGGACCTTCTTGATCGGCTTTATATTCATCATCATAAGTATCATTGCATTGAT
CTTGTGCATCTTCTACCTCATCAGGATGAACAAGTACGAGAACAAG; CDC50C –
GATGAGTGGAACGCTAAGAAAAGTTTCCAGCTTGTGAGTCTTCGTTCTATTGGTAACTCAAGTTTCAAGT
TAGCCTACGCATTCTTTCTTTTAAGTTTGTTGTATTTCATCATGATTATATTCATATTGGTTTTGGTGAAGT
GCAAGTACTATAAATTGGGTAAGACTCTTACATACTGTAAGTTATCTATGAACAAGAACATTGAGAAGAT
GAACTCAAGGAAGAAGACTAACATTCAGAACATTAACAAGAAAATAAACAGTATGCAGCTTGAGATAAT
GCATAAAGCCTCATCAGATCCTAACAATCTTGCTGGTGCTGACCACAGTCAGAAGTTGTGTTTCTGTCCA
TTGCATG. An 800-bp 5’ homology region comprising the native gene sequence upstream of the re-codonised region was cloned upstream of the SERA2loxPint. Following transfection of purified schizonts using an AMAXA nucleofector 4D (Lonza) and P3 reagent, modified parasites were selected as described previously (58).

Oligonucleotide primers used in diagnostic PCR to detect integration and excision of transgenes, and the sequences of re-codonised regions, are provided below in Tables 1 and 2.

CDC50B-HA:loxP GCα-mCherry was generated by transfection of CDC05B-HA:loxP. A linearised donor DNA which inserted mCherry in-frame with the C-terminus of GCα followed by a T2A peptide and BSD selection marker when integrated, and three pDC2-based (33) Cas9 gRNA plasmids were co-transfected, each with different sgRNA targeting the C-terminus of GCα.

sgRNA sequences as follows: sgRNA1 CTCTAAATTATTACAAAATA, sgRNA 2 AGAAAAAACATTCAAGTATC, sgRNA 3 ACGATGAAAAAAAGAAGAAG. Parasites were left to grow for two days post transfection followed by treatment with 5 µg/ml BSD to select for integrants. After the emergence of BSD resistant parasites gDNA was screened for correct integration. Donor sequences were constructed by amplifying a T2A BSD sequence from pDCIn (DiCre induction) (17) by PCR and cloning using a BsrGI site in frame with the C-terminus of a donor DNA targeting GCα which had previously been constructed in the lab (18).

Parasite sample preparation and western blot

Parasite culture supernatant samples for egress and adhesin shedding assays were prepared from tightly synchronised cultures as previously described ref. Percoll-purified mature schizonts were resuspended in complete medium and allowed to further mature for 3 h until predominantly mature segmented schizonts. The experiment was then initiated by washing parasites with RPMI three times followed by final re-suspension at a 10% haematocrit in fresh warm RPMI medium. Culture supernatant aliquots (100 µL) were harvested at specified time points by centrifugation. The schizont pellet from t = 0 was retained as a pellet control sample.

Parasite extracts were prepared from Percoll-purified schizonts treated with 0.15% w/v saponin to remove erythrocyte material. To solubilise parasite proteins, PBS-washed saponin-treated parasite pellets were resuspended in three volumes of NP-40 extraction buffer (10 mM Tris, 150 mM NaCl, 0.5 mM EDTA, 1% NP40, pH 7.5, with 1× protease inhibitors (Roche). Samples were

gently vortexed and incubated on ice for 10 min followed by centrifugation at 12,000g for 10 min at 4°C. For western blot, SDS-solubilised proteins were electrophoresed on 4%-15% Mini-PROTEAN TGX Stain-Free Protein Gels (Bio-Rad) under reducing conditions and proteins transferred to nitrocellulose membranes using a semidry Trans-Blot Turbo Transfer System (Bio-Rad). Antibody reactions were carried out in 1% skimmed milk in PBS with 0.1% Tween-20 and washed in PBS with 0.1% Tween-20. Appropriate horseradish peroxide-conjugated secondary antibodies were used, and antibody-bound washed membranes were incubated with Clarity Western ECL substrate (Bio-Rad) and visualised using a ChemiDoc (Bio-Rad).

Antibodies used for western blots presented in this work were as follows: anti-HA monoclonal antibody (mAb) 3F10 (diluted 1:2,000) (Roche); mouse anti-GAPDH mAb (1:20,000); rabbit anti-SERA5 polyclonal antibody (1:2,000); rabbit anti-mCherry (1:2000) (Abcam); rabbit anti-haemoglobin polyclonal antibody (1:2,000) (Sigma). Densitometry quantifications were performed using ImageJ.

Immunofluorescence assays

Thin blood films were fixed with 4% formaldehyde in PBS and permeabilised with PBS containing 0.1% (v/v) Triton X-100. Blocking and antibody binding was performed in PBS 3% BSA w/v at room temperature. Slides were mounted with ProLong Gold Antifade Mountant containing DAPI (Thermo Fisher Scientific). Images were acquired with a NIKON Eclipse Ti fluorescence microscope fitted with a Hamamatsu C11440 digital camera and overlaid in ICY

bioimage analysis software or Image J. Super-resolution images were acquired using a Zeiss LSM880 confocal microscope with Airyscan detector in Airyscan SR mode. Antibodies used for IFA were as follows: anti-HA monoclonal antibody (mAb) 3F10 (diluted 1:200) (Roche); mouse anti-PMV mAb (1:50); rabbit anti-ERD2 polyclonal antibody (1:2,000); rabbit anti-EXP2 polyclonal antibody (1:500) (Abcam); rabbit anti-mCherry polyclonal antibody (1:200) (Abcam).

Flow cytometry

For growth assays, synchronous ring-stage parasites were adjusted to a 0.1% parasitaemia 1% haematocrit suspension and dispensed in triplicate into six-well plates. Samples of 100 µL were harvested at days 0, 2, 4 and 6 for each well and fixed with 4% formaldehyde 0.2% glutaraldehyde in PBS. Fixed samples were stained with SYBR green and analysed by flow cytometry.

Fluorescent lipid labelling

NBD-PC, NBD-PE, NBD-PS (Avanti polar lipids) were dried and re-suspended in RPMI to 1 mM stock solutions and stored at -20°C. Relevant parasite stages (trophozoites or late schizonts) from a highly synchronous cultures were pelleted and washed twice with RPMI. Parasites were then re-suspended in RPMI containing Hoechst with 1 µM of NBD lipid or no lipid (negative control). Suspensions were incubated at 37°C for 30 minutes and subsequently pelleted by centrifugation. Pellets were then washed three times with pre-warmed RPMI containing 5%

BSA followed by resuspension in PBS. Suspensions were then diluted 1:10 and analysed by flow cytometry on an Attune NxT. Samples were gated for Hoechst DNA positivity and the resultant population gated for NBD lipid fluorescence. For trophozoite samples a low Hoechst signal population was gated, and for schizont samples a high Hoechst signal population.

Immuno-precipitation

Tightly synchronised schizonts (~45 h old) of CDC50B-HA:loxP, CDC50B-HA:loxP GCα-mCherry, CDC50C-HA:loxP and 3D7DiCre parental parasites were enriched on a 70% Percoll cushion. The schizonts were treated for 3 h with 1 µM C2 (to arrest egress) after which the cultures were treated with 0.15% saponin in PBS containing cOmplete Mini EDTA-free Protease and PhosSTOP Phosphatase inhibitor cocktails (both Roche) for 10 min at 4°C to lyse the host erythrocytes. Samples were washed twice in PBS containing protease and phosphatase inhibitors, snap-frozen and pellets stored at −80°C. Parasite pellets (70-100 µl packed volume) were resuspended in three volumes of NP-40 extraction buffer (10 mM Tris, 150 mM NaCl, 0.5 mM EDTA, 1% NP40, pH 7.5, with 1× protease inhibitors (Roche). Samples were gently vortexed and incubated on ice for 10 min followed by centrifugation at 12,000g for 10 min at 4°C. Clarified lysates were then added to anti-HA antibody conjugated magnetic beads (Thermo Scientific) or RFP trap beads (Chromotek) which had been equilibrated in NP-40 extraction buffer. Samples were incubated at room temperature for 2 h on a rotating wheel after which beads were precipitated using a magnetic sample rack. The supernatant was removed, and beads washed three times with NP-40 extraction buffer followed by three washes with extraction buffer

lacking detergent. Washed beads were then resuspended in trypsinisation buffer (50 mM ammonium bicarbonate, 40 mM 2-chloroacetamide and 10 mM Tris-(2-carboxyethyl) phosphine hydrochloride) and samples reduced and alkylated by heated to 70°C for 5 minutes. 250 ng of trypsin was added to the samples and heated at 37°C overnight with gentle agitation followed by filtration using a 0.22 µm Costar® Spin-X® centrifuge tube filter (Sigma). Samples were then run on a LTQ-Orbitrap-Velos mass spectrometer (Thermo Scientific). Search engines, Mascot (http://www.matrixscience.com/) and MaxQuant (https://www.maxquant.org/) were used for mass spectrometry data analysis. The PlasmoDB database was used for protein annotation. Peptide and proteins having minimum threshold of 95% were used for further proteomic analysis and peptide traces analysed using Scaffold4.

Measurement of hemozoin content

A culture of 5% parasitemia 1 h synchronised rings stage CDC50C parasites were treated at 1 h post invasion with DMSO or RAP (100 nM) and then left to develop until the early trophozoite stage at 36 h post-invasion. Parasites were then harvested by saponin lysis and then processed similarly to a reported method (46) to purify hemozoin. Pellets were then de-polymerised in 0.5 ml of 0.2 M NaOH solution and the resultant heme content measured by absorbance at 410 nm in a Spectramax iD5 plate reader.

Measurement of intracellular cyclic nucleotide levels

cAMP and cGMP in mature CDC50B schizonts were measured using enzyme-linked immunosorbent assay (ELISA)-based high-sensitivity direct cAMP and cGMP colorimetric assay kits (Enzo Life Sciences). Mature schizonts were Percoll purified from RAP- or DMSO-treated CDC50B-HA:loxP cultures followed by resuspension and lysis in 0.1 M HCl solution. Samples were pelleted at 10,000 × g, and the supernatant was collected and stored at –80°C until required. To perform the ELISA, samples and standards were acetylated to improve detection sensitivity according to the manufacturer's instructions. Standards and samples were run in triplicate on the same plate and absorbance at 410 nm read with a Spectramax iD5 plate reader. The standard was fitted to a sigmoidal curve and used to determine cyclic nucleotide concentrations in parasite samples. Remaining supernatant was assayed for protein concentration by a Bradford assay kit (Pierce). cGMP and cAMP reading were normalised by protein content from the Bradford assay.

Acknowledgments

We would like to thank the following for the kind gifts of antibodies used in this work: Daniel Goldberg (Washington University, St. Louis, MO) for the mouse anti-plasmepsin V mAb; Claudia Daubenberger (SwissTPH, Basel, Switzerland) for the mouse anti-GAPDH mAb; Christiaan van Ooij (LSHTM, London, UK) for the rabbit anti-EXP2 polyclonal antibody.

Author contributions

528 All experiments were designed and carried out by AP. MJB and DAB supervised the work overall
529 and SDN designed and provided plasmids for CRISPR editing of GCα.

530

531 **Funding:** This work was supported by Wellcome Trust grant 106240/Z/14/Z (to DAB),
532 Wellcome Trust grant 106239/Z/14/A (to MJB), and Wellcome ISSF2 funding to the London
533 School of Hygiene & Tropical Medicine. For the purpose of Open Access, the author has applied
534 a CC BY public copyright licence to any Author Accepted Manuscript version arising from this
535 submission. This work was also supported by funding to MJB from the Francis Crick Institute
536 (https://www.crick.ac.uk/), which receives its core funding from Cancer Research UK
537 (FC001043; https://www.cancerresearchuk.org), the UK Medical Research Council (FC001043;
538 https://www.mrc.ac.uk/), and the Wellcome Trust (FC001043; https://wellcome.ac.uk/).

539 List of abbreviations

540 ATP2 - phospholipid-transporting ATPase 2

541 ATP7 - ATPase seven

542 cAMP - cyclic AMP

543 Cas9 - CRISPR associated protein nine

544 CDC50 - cell division control protein 50

545 cGMP - cyclic GMP

546 CRISPR - clustered regularly interspersed short palindromic repeats

DiCre - dimerisable Cre-recombinase

DMSO - dimethyl sulfoxide

ERD2 - endoplasmic reticulum retention defective two

EXP2 - exported protein two

GAPDH - glyceraldehyde three phosphate dehydrogenase

GCα - guanylyl cyclase alpha

GCβ - guanylyl cyclase beta

HA3 - triple hemagglutinin epitope tag

IFA – immunofluorescence assay

mCherry - monomeric cherry fluorescent protein

MMV - Medicines for Malaria Venture

NBD-PC - nitro-benzoxadiazol phosphatidylcholine

NBD-PE - nitro-benzoxadiazol phosphatidylethanolamine

NBD-PS - nitro-benzoxadiazol phosphatidylserine

P4-ATPase - type IV ATPases

PC - phosphatidylcholine

PE - phosphatidylethanolamine

564 PMV - plasmepsin five

565 PS - phosphatidylserine

566 RAP - rapamycin

567 RFP - red fluorescent protein

568 SBP - skeleton binding protein

569 SERA5 - serine repeat antigen 5

570 sgRNA- single guide RNA

571 SLI - selection-linked integration

572

573 References

574 1. World malaria report 2021.

575 2. Balikagala B, Fukuda N, Ikeda M, Katuro OT, Tachibana S-I, Yamauchi M, Opio W, Emoto
576 S, Anywar DA, Kimura E, Palacpac NMQ, Odongo-Aginya EI, Ogwang M, Horii T, Mita T.
577 2021. Evidence of Artemisinin-Resistant Malaria in Africa. N Engl J Med 385:1163–1171.

578 3. Bannister L, Mitchell G. 2003. The ins, outs and roundabouts of malaria. Trends Parasitol
579 19:209–213.

580 4. Baillie GS, Tejeda GS, Kelly MP. 2019. Therapeutic targeting of 3',5'-cyclic nucleotide
581 phosphodiesterases: inhibition and beyond. Nat Rev Drug Discov 18:770–796.

582 5. Scott JD. 1991. Cyclic nucleotide-dependent protein kinases. Pharmacol Ther 50:123–
583 145.

584 6. Conti M, Beavo J. 2007. Biochemistry and physiology of cyclic nucleotide
585 phosphodiesterases: essential components in cyclic nucleotide signaling. Annu Rev
586 Biochem 76:481–511.

587 7. Baker DA, Drought LG, Flueck C, Nofal SD, Patel A, Penzo M, Walker EM. 2017. Cyclic
588 nucleotide signalling in malaria parasites. Open Biol 7.

589 8. Collins CR, Hackett F, Strath M, Penzo M, Withers-Martinez C, Baker DA, Blackman MJ.
590 2013. Malaria parasite cGMP-dependent protein kinase regulates blood stage merozoite
591 secretory organelle discharge and egress. PLoS Pathog 9.

592 9. Taylor CJ, McRobert L, Baker DA. 2008. Disruption of a Plasmodium falciparum cyclic
593 nucleotide phosphodiesterase gene causes aberrant gametogenesis. Mol Microbiol
594 69:110–118.

595 10. McRobert L, Taylor CJ, Deng W, Fivelman QL, Cummings RM, Polley SD, Billker O, Baker
596 DA. 2008. Gametogenesis in malaria parasites is mediated by the cGMP-dependent
597 protein kinase. PLoS Biol 6:1243–1252.

598 11. Falae A, Combe A, Amaladoss A, Carvalho T, Menard R, Bhanot P. 2010. Role of
599 Plasmodium berghei cGMP-dependent protein kinase in late liver stage development. J
600 Biol Chem 285:3282–3288.

601 12. Govindasamy K, Jebiwott S, Jaijyan DK, Davidow A, Ojo KK, Van Voorhis WC, Brochet M,

Billker O, Bhanot P. 2016. Invasion of hepatocytes by Plasmodium sporozoites requires cGMP-dependent protein kinase and calcium dependent protein kinase 4. Mol Microbiol 102:349–363.

13. Ishino T, Orito Y, Chinzei Y, Yuda M. 2006. A calcium-dependent protein kinase regulates Plasmodium ookinete access to the midgut epithelial cell. Mol Microbiol 59:1175–1184.

14. Moon RW, Taylor CJ, Bex C, Schepers R, Goulding D, Janse CJ, Waters AP, Baker DA, Billker O. 2009. A cyclic GMP signalling module that regulates gliding motility in a malaria parasite. PLoS Pathog 5.

15. Ono T, Cabrita-Santos L, Leitao R, Bettiol E, Purcell LA, Diaz-Pulido O, Andrews LB, Tadakuma T, Bhanot P, Mota MM, Rodriguez A. 2008. Adenylyl cyclase alpha and cAMP signaling mediate Plasmodium sporozoite apical regulated exocytosis and hepatocyte infection. PLoS Pathog 4.

16. Ramdani G, Naissant B, Thompson E, Breil F, Lorthiois A, Dupuy F, Cummings R, Duffier Y, Corbett Y, Mercereau-Puijalon O, Vernick K, Taramelli D, Baker D a, Langsley G, Lavazec C. 2015. cAMP-Signalling Regulates Gametocyte-Infected Erythrocyte Deformability Required for Malaria Parasite Transmission. PLoS Pathog 11:e1004815.

17. Patel A, Perrin AJ, Flynn HR, Bisson C, Withers-Martinez C, Treeck M, Flueck C, Nicastro G, Martin SR, Ramos A, Gilberger TW, Snijders AP, Blackman MJ, Baker DA. 2019. Cyclic AMP signalling controls key components of malaria parasite host cell invasion machinery. PLoS Biol 17.

622 18. Nofal SD, Patel A, Blackman MJ, Flueck C, Baker DA. 2021. Plasmodium falciparum
623 Guanylyl Cyclase-Alpha and the Activity of Its Appended P4-ATPase Domain Are Essential
624 for cGMP Synthesis and Blood-Stage Egress. MBio 12:1–19.

625 19. Carucci DJ, Witney a a, Muhia DK, Warhurst DC, Schaap P, Meima M, Li JL, Taylor MC,
626 Kelly JM, Baker D a. 2000. Guanylyl cyclase activity associated with putative bifunctional
627 integral membrane proteins in Plasmodium falciparum. J Biol Chem 275:22147–56.

628 20. Gao H, Yang Z, Wang X, Qian P, Hong R, Chen X, Su X zhuan, Cui H, Yuan J. 2018. ISP1-
629 Anchored Polarization of GCβ/CDC50A Complex Initiates Malaria Ookinete Gliding
630 Motility. Curr Biol 28:2763-2776.e6.

631 21. Best JT, Xu P, Graham TR. 2019. Phospholipid flippases in membrane remodeling and
632 transport carrier biogenesis. Curr Opin Cell Biol 59:8–15.

633 22. Bisio H, Lunghi M, Brochet M, Soldati-Favre D. 2019. Phosphatidic acid governs natural
634 egress in Toxoplasma gondii via a guanylate cyclase receptor platform. Nat Microbiol
635 4:420–428.

636 23. Brown KM, Sibley LD. 2018. Essential cGMP Signaling in Toxoplasma Is Initiated by a
637 Hybrid P-Type ATPase-Guanylate Cyclase. Cell Host Microbe 24:804-816.e6.

638 24. Yang L, Uboldi AD, Seizova S, Wilde ML, Coffey MJ, Katris NJ, Yamaryo-Botté Y, Kocan M,
639 Bathgate RAD, Stewart RJ, McConville MJ, Thompson PE, Botté CY, Tonkin CJ. 2019. An
640 apically located hybrid guanylate cyclase-ATPase is critical for the initiation of Ca 2+
641 signaling and motility in Toxoplasma gondii. J Biol Chem 294:8959–8972.

642 25. Günay-Esiyok O, Scheib U, Noll M, Gupta N. 2019. An unusual and vital protein with
643 guanylate cyclase and P4-ATPase domains in a pathogenic protist. Life Sci alliance 2.

644 26. Saito K, Fujimura-Kamada K, Futura N, Kato U, Umeda M, Tanaka K. 2004. Cdc50p, a
645 protein required for polarized growth, associates with the Drs2p P-type ATPase
646 implicated in phospholipid translocation in Saccharomyces cerevisiae. Mol Biol Cell
647 15:3418–3432.

648 27. Chen S, Wang J, Muthusamy BP, Liu K, Zare S, Andersen RJ, Graham TR. 2006. Roles for
649 the Drs2p-Cdc50p complex in protein transport and phosphatidylserine asymmetry of
650 the yeast plasma membrane. Traffic 7:1503–1517.

651 28. Timcenko M, Lyons JA, Januliene D, Ulstrup JJ, Dieudonné T, Montigny C, Ash MR, Karlsen
652 JL, Boesen T, Kühlbrandt W, Lenoir G, Moeller A, Nissen P. 2019. Structure and
653 autoregulation of a P4-ATPase lipid flippase. Nature 571:366–370.

654 29. Hiraizumi M, Yamashita K, Nishizawa T, Nureki O. 2019. Cryo-EM structures capture the
655 transport cycle of the P4-ATPase flippase. Science 365:1149–1155.

656 30. Lenoir G, Williamson P, Puts CF, Holthuis JCM. 2009. Cdc50p plays a vital role in the
657 ATPase reaction cycle of the putative aminophospholipid transporter Drs2p. J Biol Chem
658 284:17956–17967.

659 31. Bryde S, Hennrich H, Verhulst PM, Devaux PF, Lenoir G, Holthuis JCM. 2010. CDC50
660 proteins are critical components of the human class-1 P4-ATPase transport machinery. J
661 Biol Chem 285:40562–40572.

662 32. Collins CR, Das S, Wong EH, Andenmatten N, Stallmach R, Hackett F, Herman JP, Müller S,
663 Meissner M, Blackman MJ. 2013. Robust inducible Cre recombinase activity in the human
664 malaria parasite Plasmodium falciparum enables efficient gene deletion within a single
665 asexual erythrocytic growth cycle. Mol Microbiol 88:687–701.

666 33. Knuepfer E, Napiorkowska M, Van Ooij C, Holder AA. 2017. Generating conditional gene
667 knockouts in Plasmodium - a toolkit to produce stable DiCre recombinase-expressing
668 parasite lines using CRISPR/Cas9. Sci Rep 7.

669 34. Toenhake CG, Fraschka SAK, Vijayabaskar MS, Westhead DR, van Heeringen SJ, Bártfai R.
670 2018. Chromatin Accessibility-Based Characterization of the Gene Regulatory Network
671 Underlying Plasmodium falciparum Blood-Stage Development. Cell Host Microbe 23:557-
672 569.e9.

673 35. Yeoh S, O'Donnell RA, Koussis K, Dluzewski AR, Ansell KH, Osborne SA, Hackett F,
674 Withers-Martinez C, Mitchell GH, Bannister LH, Bryans JS, Kettleborough CA, Blackman
675 MJ. 2007. Subcellular discharge of a serine protease mediates release of invasive malaria
676 parasites from host erythrocytes. Cell 131:1072–1083.

677 36. Salowe SP, Wiltsie J, Liberator PA, Donald RGK. 2002. The role of a parasite-specific
678 allosteric site in the distinctive activation behavior of Eimeria tenella cGMP-dependent
679 protein kinase. Biochemistry 41:4385–4391.

680 37. Paul AS, Miliu A, Paulo JA, Goldberg JM, Bonilla AM, Berry L, Seveno M, Braun-Breton C,
681 Kosber AL, Elsworth B, Arriola JSN, Lebrun M, Gygi SP, Lamarque MH, Duraisingh MT.
682 2020. Co-option of Plasmodium falciparum PP1 for egress from host erythrocytes. Nat

683 Commun 11.

684 38. Poulsen LR, López-Marqués RL, Pedas PR, McDowell SC, Brown E, Kunze R, Harper JF,
685 Pomorski TG, Palmgren M. 2015. A phospholipid uptake system in the model plant
686 Arabidopsis thaliana. Nat Commun 6.

687 39. Pomorski T, Lombardi R, Riezman H, Devaux PF, Van Meer G, Holthuis JCM. 2003. Drs2p-
688 related P-type ATPases Dnf1p and Dnf2p are required for phospholipid translocation
689 across the yeast plasma membrane and serve a role in endocytosis. Mol Biol Cell
690 14:1240–1254.

691 40. Pomorski T, Holthuis JCM, Hermann A, van Meer G. 2004. Tracking down lipid flippases
692 and their biological functions. J Cell Sci 117:805–813.

693 41. Poulsen LR, López-Marqués RL, McDowell SC, Okkeri J, Licht D, Schulz A, Pomorski T,
694 Harper JF, Palmgren MG. 2008. The Arabidopsis P4-ATPase ALA3 localizes to the golgi
695 and requires a beta-subunit to function in lipid translocation and secretory vesicle
696 formation. Plant Cell 20:658–676.

697 42. Harsay E, Bretscher A. 1995. Parallel secretory pathways to the cell surface in yeast. J Cell
698 Biol 131:297–310.

699 43. Pomorski T, Lombardi R, Riezman H, Devaux PF, Van Meer G, Holthuis JCM. 2003. Drs2p-
700 related P-type ATPases Dnf1p and Dnf2p are required for phospholipid translocation
701 across the yeast plasma membrane and serve a role in endocytosis. Mol Biol Cell
702 14:1240–1254.

703 44. Gall WE, Geething NC, Hua Z, Ingram MF, Liu K, Chen SI, Graham TR. 2002. Drs2p-
704 dependent formation of exocytic clathrin-coated vesicles in vivo. Curr Biol 12:1623–1627.

705 45. Elsworth B, Matthews K, Nie CQ, Kalanon M, Charnaud SC, Sanders PR, Chisholm SA,
706 Counihan NA, Shaw PJ, Pino P, Chan JA, Azevedo MF, Rogerson SJ, Beeson JG, Crabb BS,
707 Gilson PR, De Koning-Ward TF. 2014. PTEX is an essential nexus for protein export in
708 malaria parasites. Nature 511:587–591.

709 46. Coban C, Ishii KJ, Sullivan DJ, Kumar N. 2002. Purified malaria pigment (hemozoin)
710 enhances dendritic cell maturation and modulates the isotype of antibodies induced by a
711 DNA vaccine. Infect Immun 70:3939–3943.

712 47. Bushkin GG, Ratner DM, Cui J, Banerjee S, Duraisingh MT, Jennings C V., Dvorin JD,
713 Gubbels MJ, Robertson SD, Steffen M, O'Keefe BR, Robbins PW, Samuelson J. 2010.
714 Suggestive evidence for Darwinian Selection against asparagine-linked glycans of
715 Plasmodium falciparum and Toxoplasma gondii. Eukaryot Cell 9:228–241.

716 48. Lamy A, Macarini-Bruzaferro E, Dieudonné T, Perálvarez-Marín A, Lenoir G, Montigny C,
717 le Maire M, Vázquez-Ibar JL. 2021. ATP2, The essential P4-ATPase of malaria parasites,
718 catalyzes lipid-stimulated ATP hydrolysis in complex with a Cdc50 β-subunit. Emerg
719 Microbes Infect 10:132–147.

720 49. Zhang M, Wang C, Otto TD, Oberstaller J, Liao X, Adapa SR, Udenze K, Bronner IF,
721 Casandra D, Mayho M, Brown J, Li S, Swanson J, Rayner JC, Jiang RHY, Adams JH. 2018.
722 Uncovering the essential genes of the human malaria parasite Plasmodium falciparum by
723 saturation mutagenesis. Science 360.

50. Kenthirapalan S, Waters AP, Matuschewski K, Kooij TWA. 2016. Functional profiles of orphan membrane transporters in the life cycle of the malaria parasite. Nat Commun 7:10519.

51. Cowell AN, Istvan ES, Lukens AK, Gomez-Lorenzo MG, Vanaerschot M, Sakata-Kato T, Flannery EL, Magistrado P, Owen E, Abraham M, La Monte G, Painter HJ, Williams RM, Franco V, Linares M, Arriaga I, Bopp S, Corey VC, Gnädig NF, Coburn-Flynn O, Reimer C, Gupta P, Murithi JM, Moura PA, Fuchs O, Sasaki E, Kim SW, Teng CH, Wang LT, Akidil A, Adjalley S, Willis PA, Siegel D, Tanaseichuk O, Zhong Y, Zhou Y, Llinás M, Ottilie S, Gamo FJ, Lee MCS, Goldberg DE, Fidock DA, Wirth DF, Winzeler EA. 2018. Mapping the malaria parasite druggable genome by using in vitro evolution and chemogenomics. Science 359:191–199.

52. Goldberg DE. 1993. Hemoglobin degradation in Plasmodium-infected red blood cells. Semin Cell Biol 4:355–361.

53. Xie SC, Ralph SA, Tilley L. 2020. K13, the Cytostome, and Artemisinin Resistance. Trends Parasitol 36:533–544.

54. Yang Z, Shi Y, Cui H, Yang S, Gao H, Yuan J. 2021. A malaria parasite phospholipid flippase safeguards midgut traversal of ookinetes for mosquito transmission. Sci Adv 7.

55. Bisio H, Krishnan A, Marq J-B, Soldati-Favre D. 2021. Toxoplasma gondii phosphatidylserine flippase complex ATP2B-CDC50.4 critically participates in microneme exocytosis. bioRxiv 2021.11.25.470034.

744 56. Harris PK, Yeoh S, Dluzewski AR, O'Donnell RA, Withers-Martinez C, Hackett F, Bannister
745 LH, Mitchell GH, Blackman MJ. 2005. Molecular identification of a malaria merozoite
746 surface sheddase. PLoS Pathog 1:0241–0251.

747 57. Jones ML, Das S, Belda H, Collins CR, Blackman MJ, Treeck M. 2016. A versatile strategy
748 for rapid conditional genome engineering using loxP sites in a small synthetic intron in
749 Plasmodium falciparum. Sci Rep 6:21800.

750 58. Birnbaum J, Flemming S, Reichard N, Soares AB, Mesén-Ramírez P, Jonscher E, Bergmann
751 B, Spielmann T. 2017. A genetic system to study Plasmodium falciparum protein function.
752 Nat Methods 14:450–456.

753 59. Krogh A, Larsson B, Von Heijne G, Sonnhammer ELL. 2001. Predicting transmembrane
754 protein topology with a hidden Markov model: application to complete genomes. J Mol
755 Biol 305:567–580.

756

757 Figure legends

758 (1A) Representation of the three CDC50 proteins in *P. falciparum* displayed from N- to C-
759 terminus in a relative scale. White boxes indicate transmembrane helices (TMDs) as predicted
760 by the TMHMM server (59). Arrows indicate the point at which the protein products are
761 truncated when the corresponding modified locus is excised in transgenically-modified parasite
762 lines. For CDC50A this is from Phe341, for CDC50B His235 and CDC50C from Glu383.

763

764 (1B) Schematic representation of the SLI strategy (58) used to produce the three CDC50 DiCre
765 lines and resultant RAP-induced disruption of the modified genes. Double-headed arrows
766 represent the regions amplified by PCR in (1C). Red arrowheads represent *loxP* sites, yellow
767 lollipops represent translational stop codons, white boxes indicate TMDs and light blue boxes
768 indicate regions of re-codonised sequence (R.R.).

769

770 (1C) Diagnostic PCR analysis of gDNA from transgenic CDC50 parasite lines verifying successful
771 modification of target loci by SLI to produce CDC50A-HA:loxP, CDC50B-HA:loxP and CDC50C-
772 HA:loxP. Efficient excision of 'floxed' sequences is observed upon treatment with RAP for all
773 lines. Track C represents amplification of a control locus (PKAc) to check gDNA integrity. PCRs 1-
774 4 are represented in the schematic locus in panel 1B. PCR 1 screens for the WT locus, PCR 2 for
775 5' integration, PCR 3 for 3' integration and PCR 4 for the excision of the 'floxed' sequence. See
776 Table 1 for sequences of all primers used for PCR. Sizes for expected amplification products are
777 as follows: C, control locus (primers 16 and 17) 1642b.p. CDC50A; PCR 1 (primers 21 and 22)
778 1842b.p, PCR2 (primers 21 and 18) 1613b.p, PCR3 (primers 20 and 22) 1670b.p and PCR 4
779 (primers 21 and 19) 2863b.p (DMSO), 1169b.p (RAP). CDC50B; PCR 1 (primers 23 and 24)
780 1423b.p, PCR2 (primers 23 and 18) 1457b.p, PCR3 (primers 20 and 24) 1321b.p and PCR 4
781 (primers 23 and 19) 2707b.p (DMSO), 1010b.p (RAP). CDC50C; PCR 1 (primers 25 and 26)
782 1369b.p, PCR2 (primers 25 and 18) 1602b.p, PCR3 (primers 20 and 26) 1172b.p and PCR 4
783 (primers 25 and 19) 2852b.p (DMSO), 1369b.p (RAP).

784

785 (1D) Western blot analysis of expression (DMSO) and ablation (RAP) of CDC50A-HA, CDC50B-HA
786 and CDC50C-HA from highly synchronous late stage schizonts in the respective transgenic
787 parasite lines. Expression of GAPDH (PF3D7_1462800) is shown as a loading control. No
788 expression of CDC50A-HA was detected. Predicted molecular weights of CDC50B-HA, CDC50C-
789 HA and GAPDH are indicated.

790

791 (1E) IFA analysis showing the diffuse peripheral localisation of CDC50B-HA and CDCD50C-HA
792 and the loss of expression upon RAP treatment. Over 99% of all RAP-treated CDC50B-HA:loxP
793 and CDC50C-HA:loxP schizonts examined by IFA were diminished in HA expression in three
794 independent experiments. Scale bar, 2 µm.

795

796 (2A) Growth curves showing parasitaemia as measured by flow cytometry of CDC50A-HA:loxP,
797 CDC50B-HA:loxP and CDC50C-HA:loxP parasites treated with DMSO (vehicle only control) or
798 RAP. Means from 3 biological replicates are plotted. Error bars, SD.

799

800 (2B) Giemsa-stained thin blood films showing ring-stage parasites following egress of
801 synchronous DMSO and RAP-treated CDC50C-HA:loxP schizonts. Ring formation occurs in RAP-
802 treated CDC50C-HA parasites, but the parasites did not develop beyond the early trophozoite
803 stage and eventually collapsed into small vacuoles.

804

(3A) Western blots demonstrate efficient immunoprecipitation (IP) of CDC50B-HA and CDC50C-HA from schizont extracts. Large black arrows indicate the predicted mass of each protein. Images are representative of 2 biological repeats.

(3B) Mass spectrometric identification of interacting partners of CDC50B and CDC50C. Volcano plot of P values versus the corresponding $\log_2$ fold change in abundance compared to 3D7DiCre control samples (Fischer's exact test). Plotted by analysing proteins enriched through IP (panel 3A) by mass spectrometry. Green line indicates $p=-2\log_{10}$ and green dots represent peptides where $p<-2\log_{10}$. Peptides for GCα and ATP2 were enriched to $p<-19\log_{10}$.

(4A) Western blot analysis monitoring egress kinetics of DMSO- and RAP-treated CDC50B-HA:loxP schizonts. The diminished detection of the SERA5 p50 proteolytic fragment in culture supernatants of RAP-treated CDC50B-HA:loxP parasites indicates an impaired egress rate in the absence of CDC50B-HA. Lower panel left, histograms of DNA (SYBR green) staining of CDC50B DMSO- or RAP-treated schizonts. 10,000 cells were counted per treatment. Image representative of 3 biological repeats. Lower panel right, Giemsa-stained thin blood films of Percoll-purified CDC50B DMSO-and RAP-treated schizonts. No delay in schizont maturation is evident in RAP-treated parasites. Images representative of 3 biological repeats Scale bar, 5µm.

824 (4B) Western blot analysis of DMSO- and RAP-treated CDC50B-HA:loxP GCα-mCherry and
825 control 3D7DiCre schizonts. The top panel shows a ~250 kDa fragment detected by an mCherry
826 antibody that is absent in control (untagged) schizont lysates. The lower panel shows the same
827 samples probed with an anti-HA antibody and an anti-GAPDH (PF3D7_1462800) loading control
828 antibody.

829

830 (4C) Immuno-precipitation of GCα-mCherry. Samples were loaded in duplicate and probed for
831 mCherry (left panel) and HA epitope (left panel). * denotes the ~40 kDa degradation product of
832 GCα-mCherry observed after enrichment and boiling of the RFP-trap beads, suggesting that
833 GCα was prone to proteolysis under the conditions used to promote binding or degrades when
834 heated.

835

836 (4D) IFA showing the localisation of CDC50B and GCα mCherry in RAP and DMSO treated
837 schizonts, top panel. Bottom panel, localisation of GCα mCherry and PMV (PF3D7_1323500), an
838 ER marker in RAP- and DMSO-treated schizonts. Scale bar, 2 µm.

839

840 (4E) Quantification of cyclic nucleotide levels in tightly synchronised DMSO- and RAP-treated
841 CDC50B mature schizonts by direct ELISA. Means are shown from 3 biological repeats plotted,
842 error bars, SD. n.s = not significant, * $P<0.05$, Student's t test.

843

844 (4F) Restoration of egress of RAP-treated CDC50B schizonts by treatment with zaprinast or PET-
845 cGMP. Supernatant and pellet samples were taken at time point 0 post washing with RPMI to
846 control for parasite numbers and egress. Samples were then taken at 60 min post incubation at
847 37 ^{o}C. -C represents no treatment. Image is representative of 3 biological repeats.

848

849 (5A) Airyscan confocal analysis of IFAs of CDC50-C trophozoites co-localised with EXP2
850 (PF3D7_1471100) an exported PV protein, ERD2 a Golgi marker (PF3D7_1353600) and PMV an
851 ER marker (PF3D7_1323500). Scale bar, 2 µm.

852

853 (5B) Flow cytometry analysis of fluorescent lipid uptake in live WT (DMSO) and CDC50C null
854 (RAP) trophozoites labelled at 36 h post invasion. Histograms are overlayed each representing
855 10,000 cells for each treatment. Cells were gated for DNA content and further for green
856 fluorescence. No detectable shift in histogram curves was seen for each lipid in RAP-treated
857 samples. Data are representative of one of three biological repeats, each of which showed the
858 same outcome. Control samples, with no lipid added, were analysed to validate the gating
859 protocol for lipid signal. Right panel shows examples of the stained cells visualised by
860 fluorescence microscopy. Scale bar 2 µm.

861

(6A) IFA imaging of DMSO- and RAP-treated CDC50C-HA:loxP trophozoites fixed at 36 h post invasion indicates no defect in export of skeleton binding protein (SBP). Right, western blot showing absence of CDC50C-HA in RAP-treated trophozoites. Scale bar, 2 µm.

(6B) Quantification of SBP puncta in DMSO- and RAP-treated CDC50C trophozoites. 66 parasites were counted from 2 individual biological replicates for SBP puncta in ImageJ. Mean values are plotted. Error bars, SD. n.s = not significant, Student's t test.

(6C) CDC50 null parasites produce smaller hemozoin crystals. Thin blood films were made from tightly synchronized DMSO- and RAP-treated CDC50C at 36 h post invasion. Inset, length of the hemozoin crystal (measurement 1) and parasite (measurement 2) were performed in ImageJ on imaged Giemsa-stained smears of DMSO- and RAP-treated CDC50C trophozoites. A ratio of crystal length to parasite length was derived by dividing measurement 1 by measurement 2. In total 46 parasites were measured from 3 independent biological repeats of CDC50B excision or control treatment. Mean values are plotted. Error bars, SD. * $P<0.05$, Student's t test.

(6D) Spectrophometric quantification of hemozoin content of CDC50C WT (DMSO) and null (RAP) trophozoites. Highly synchronised CDC50C ring stage cultures were treated with DMSO (control) or RAP. Cultures were then harvested at 36 h post invasion. Hemozoin was purified

881 using established methods (46) and quantified by absorbance at 410 nm. Means are plotted for
882 3 independent biological repeats. Error bars, SD. n.s = not significant, * P<0.05, Student's t test.

883

884 (6E) Western blot analysis of the haemoglobin content of saponin lysed CDC50-C WT and null
885 trophozoites. Highly synchronised CDC50C ring stage cultures were treated with DMSO control
886 or RAP. Cultures were then harvested at 36 h post invasion. Lysates were probed for the
887 presence of CDC50-C by HA staining. Haemoglobin content was probed alongside GAPDH as a
888 loading control. Data representative of 3 biological repeats.

889 **Table 1 – oligonucleotide primers used in this study**

	Name	Sequence
1	CDC50A 5HR F	GCGGCCGCAGATCTCTCGAGCGATATTGGACACCAAATTGTTTA
2	CDC50A 5HR R	CGAAGTTATTGTATATTATTTTTTTTATTTACCTACATGTGATTTATGTAATT CCATTTC
3	CDC50A reco F	GTATATATATATATATTTATATATTTTATATTCTTTTAGATTTCTGGCTCATG AACGAAAAGTACAAGAACGCATTAAACATG
4	CDC50A reco R	CAGATCCGCCTGAACCGGATCCCAAGAAGAAGAAGATGTAAATATAAG
5	CDC50B 5HR F	GCGGCCGCAGATCTCTCGAGTGAGTAATCTTAAAAATGACATGTTTATATC
6	CDC50B 5HR R	CGAAGTTATTGTATATTATTTTTTTTATTTACCTTTATATAATTGTACATTTT GAGGTG
7	CDC50B reco F	GTATATATATATATATTTATATATTTTATATTCTTTTAGATCACATTTACTTTT GGATGGAGC
8	CDC50B reco R	CAGATCCGCCTGAACCGGATCCCTTGTTCTCGTACTTGTTCATC
9	CDC50C reco F	GTATATATATATATATTTATATATTTTATATTCTTTTAGATGAGTGGAACGC TAAGAAAAGTTTC
10	CDC50C reco R	CCGCCTGAACCGGATCCATGCAATGGACAGAAACACAACTTC
11	CDC50C 5HR F	GATCTCTCGAGCCAGAGTACGAATTCATGAATGCTTTTAAACAACAAG
12	CDC50C 5HR R	CGAAGTTATTGTATATTATTTTTTTTATTTACCTGCTGGCCATACGTTTTGAA G
13	5HR seq F	CAGCTATGACCATGATTACGCC
14	Reco seq F	CATTATACGAAGTTATTATATATGTATATATATATATATTTATATATTTTATA TTC
16	PKAc screen F	GAAGGACAGTGATTCTAGTGAACAG
17	PKAc WT screen R	CAATTTCTTCATCAAATGTTTGCAATTGTTATC

18	HA R	GCATAGTCAGGAACATCGTAAGG
19	Exi R	CCGTTCAAATCTTCTTCAGAAATCAAC
20	3' int F	CAGCTATGACCATGATTACGCC
21	CDC50A 5' int F	CTTTAGATTATGATGATAATTTTTTGGAAGAAAAG
22	CDC50A WT R	GTGTATATTTAAAAATCAGGATTTTACTATATCCTC
23	CDC50B 5' int F	CAGTTATGTGTCTTCCCTTTGTATTATTTTG
24	CDC50B WT R	CTTTTGGTTATTAAATGTGTATCGAAATAATAC
25	CDC50C 5' int F	GTCGCAGTTCATGGGAAGG
26	CDC50C WT R	GGGAATGGTCTGCTCCTGCT
27	T2A BSD amp F	GCGGCATGGACGAGCTGTACAAGAGTGGAGAAGGAAGAGG
28	T2A BSD amp R	GTGTTGATGGTTTTGGGCTAGCTTAGCCCTCCCACACATAACC
29	Screen T2A F	CGAGGACTACACCATCGTGG
30	GCtag WT F	CTAAGAATATTCATTCCTACGATG
31	GCtag 3' int F	CAATGGCACCTTTGTCTCAAG
32	GCtag 5' int F	CATGGGCAAATGGTGTAGATG
33	GCtag 5' int R	CCTCCATGTGCACCTTG
34	GCtag WT R	CGAATGTTCGGAAAAATATTCATGTGC
35	p230p Int screen F	CTATATGGTATCCAAAACCTTTAAATTATATAGC
36	p230p WT screen R	GAGGAATTTTTAAATATGATATACCTTTATCATTAG

890

Figure 1

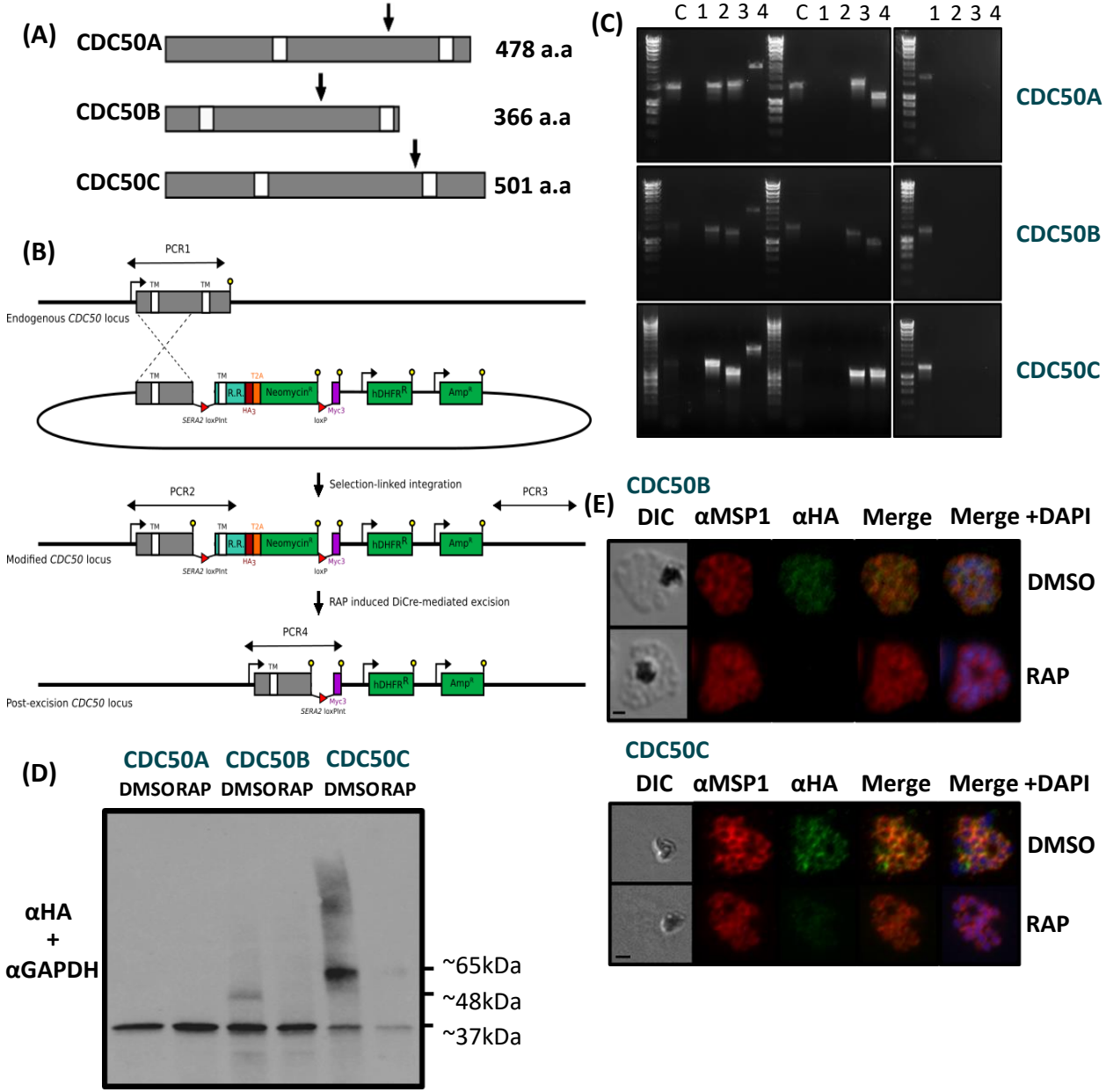
(A)
CDC50A
478 a.a
CDC50B
366 a.a
CDC50C
501 a.a
(B)
PCR1
Endogenous CDC50 locus
Selection-linked integration
PCR2
PCR3
Modified CDC50 locus
RAP induced DiCre-mediated excision
PCR4
Post-excision CDC50 locus
(C)
DMSO
RAP
3D7 DiCre
C 1 2 3 4 C 1 2 3 4 1 2 3 4
CDC50A
CDC50B
CDC50C
(D)
CDC50A CDC50B CDC50C
DMSORAP DMSORAP DMSORAP
αHA
+
αGAPDH
~65kDa
~48kDa
~37kDa
(E)
CDC50B
DIC αMSP1 αHA Merge Merge +DAPI
DMSO
RAP
CDC50C
DIC αMSP1 αHA Merge Merge +DAPI
DMSO
RAP

Figure 2

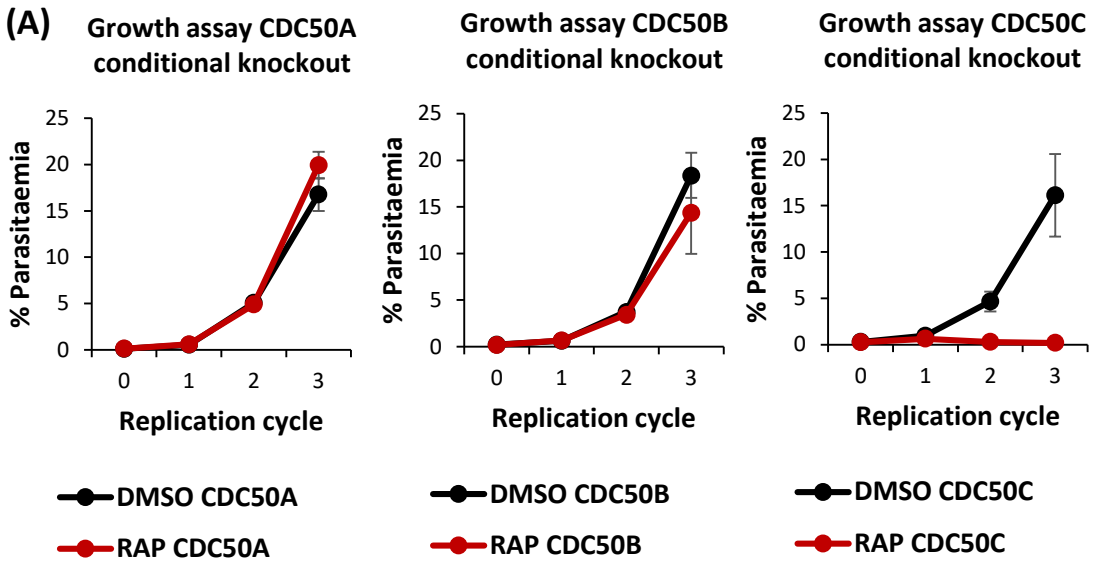
(A)
Growth assay CDC50A conditional knockout
Growth assay CDC50B conditional knockout
Growth assay CDC50C conditional knockout
% Parasitaemia
Replication cycle
DMSO CDC50A
RAP CDC50A
DMSO CDC50B
RAP CDC50B
DMSO CDC50C
RAP CDC50C

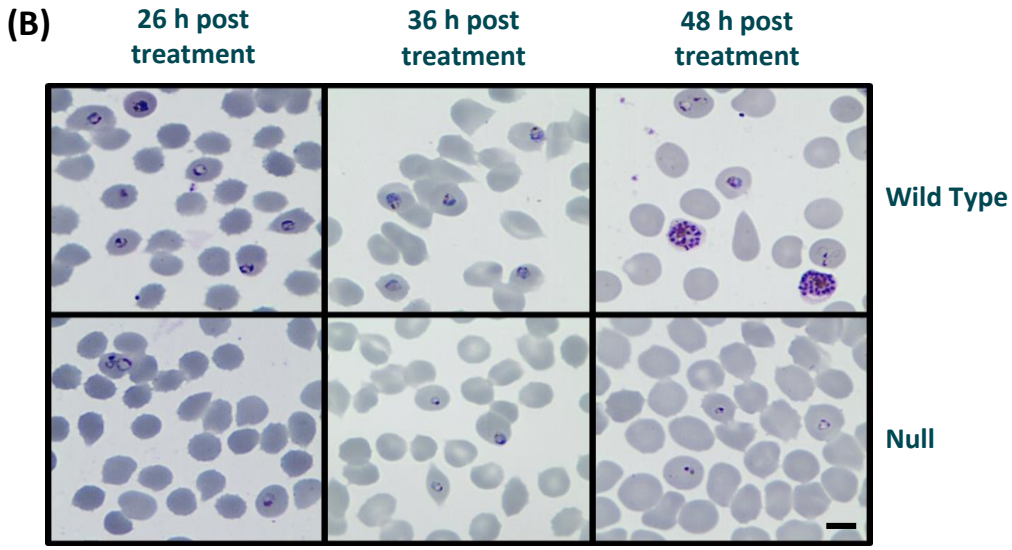
(B)
26 h post treatment
36 h post treatment
48 h post treatment
Wild Type
Null

Figure 3

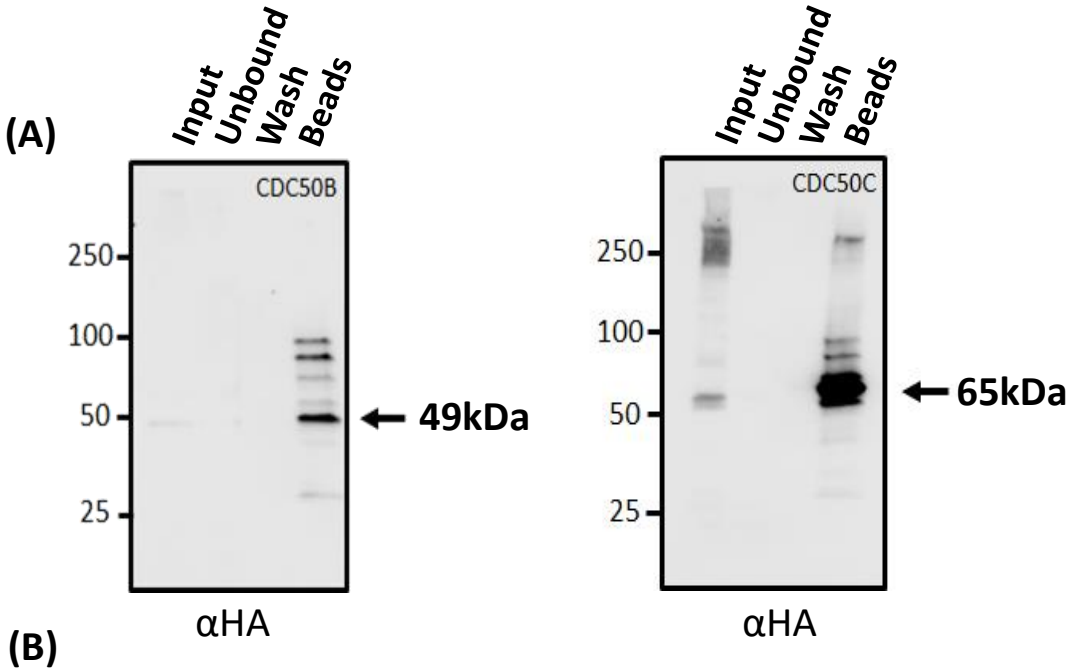
(A)
Input
Unbound
Wash
Beads
CDC50B
250
100
50
25
49kDa
αHA
Input
Unbound
Wash
Beads
CDC50C
250
100
50
25
65kDa
αHA

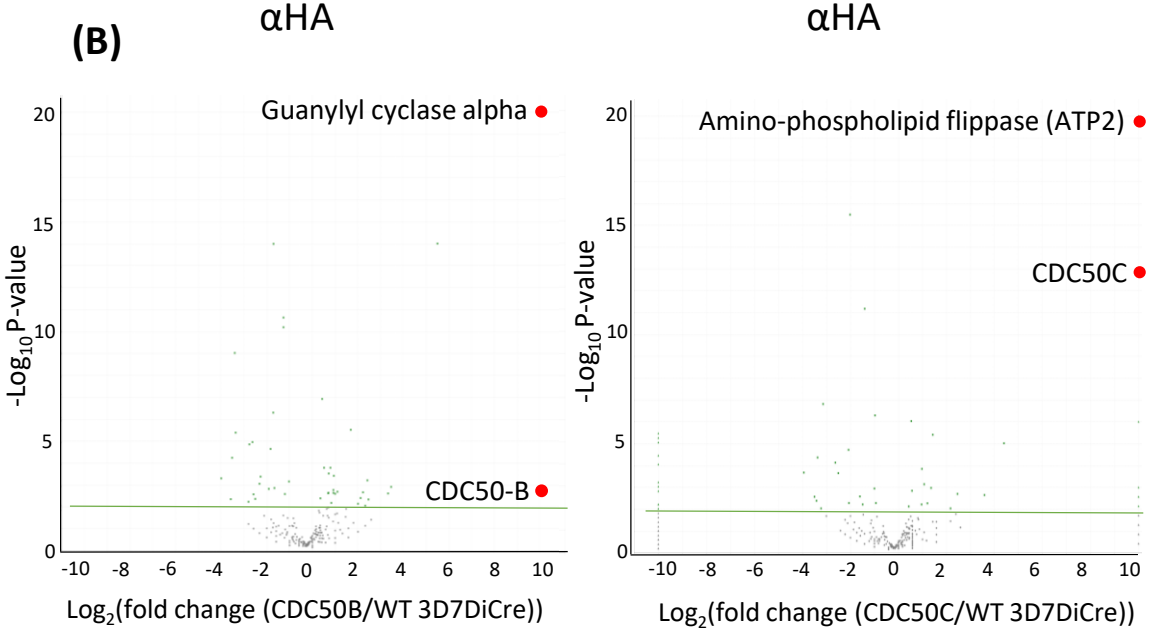
(B)
Guanylyl cyclase alpha
CDC50-B
-Log10 P-value
Log2(fold change (CDC50B/WT 3D7DiCre))
Amino-phospholipid flippase (ATP2)
CDC50C
-Log10 P-value
Log2(fold change (CDC50C/WT 3D7DiCre))

Figure 4

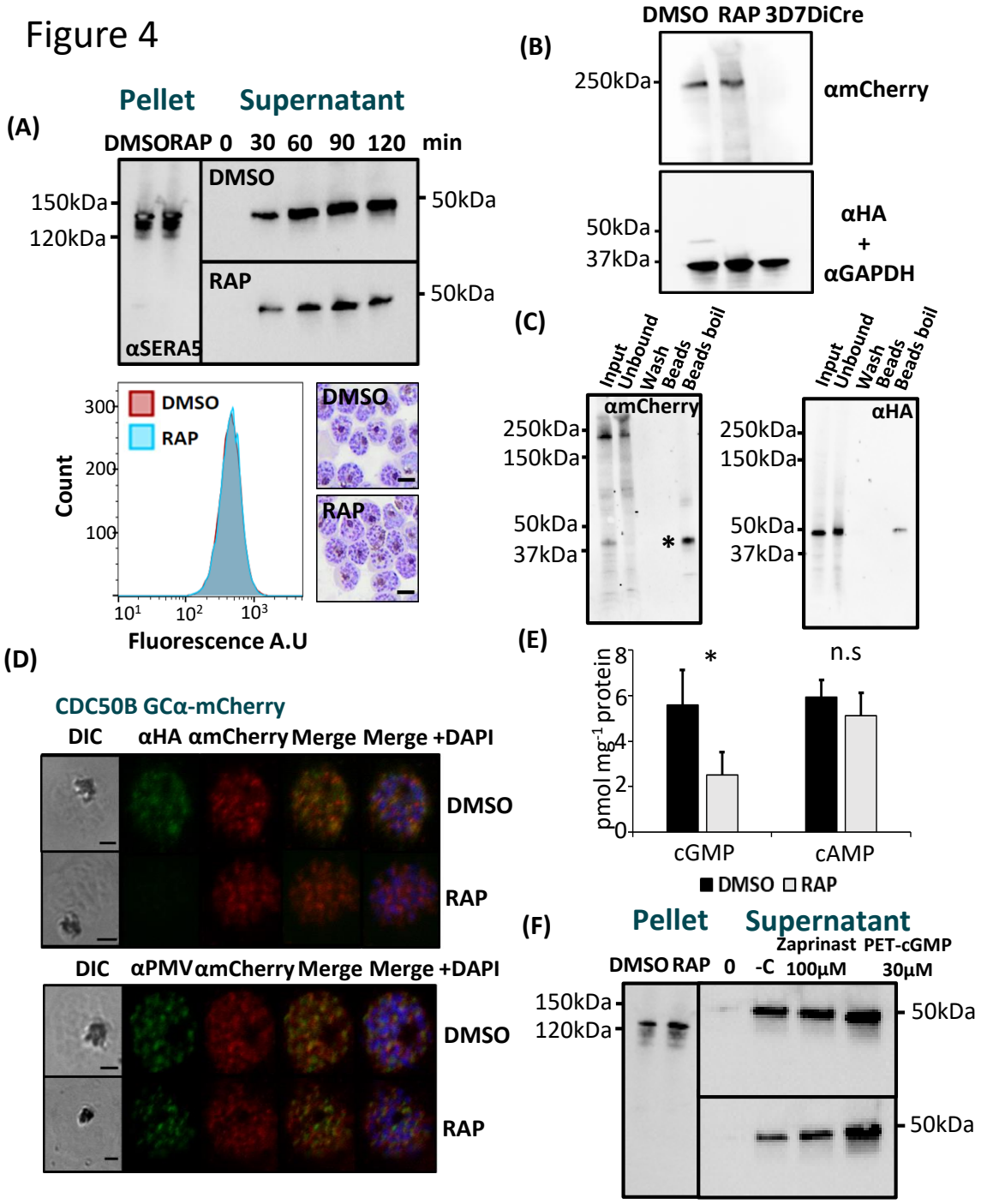
(A)
Pellet
Supernatant
DMSO RAP 0 30 60 90 120 min
150kDa
120kDa
DMSO
RAP
50kDa
50kDa
αSERA5
300
200
100
Count
DMSO
RAP
10^1 10^2 10^3
Fluorescence A.U
DMSO
RAP
(B)
DMSO RAP 3D7DiCre
250kDa
αmCherry
50kDa
37kDa
αHA
+
αGAPDH
(C)
Input Unbound Wash Beads Beads boil
αmCherry
250kDa
150kDa
50kDa
37kDa
*
αHA
(D)
CDC50B GCα-mCherry
DIC αHA αmCherry Merge Merge +DAPI
DMSO
RAP
DIC αPMV αmCherry Merge Merge +DAPI
DMSO
RAP
(E)
pmol mg-1 protein
8
6
4
2
0
*
n.s
cGMP
cAMP
DMSO RAP
(F)
Pellet
Supernatant
DMSO RAP 0
Zaprinast PET-cGMP
-C 100μM 30μM
150kDa
120kDa
50kDa
50kDa

Figure 5

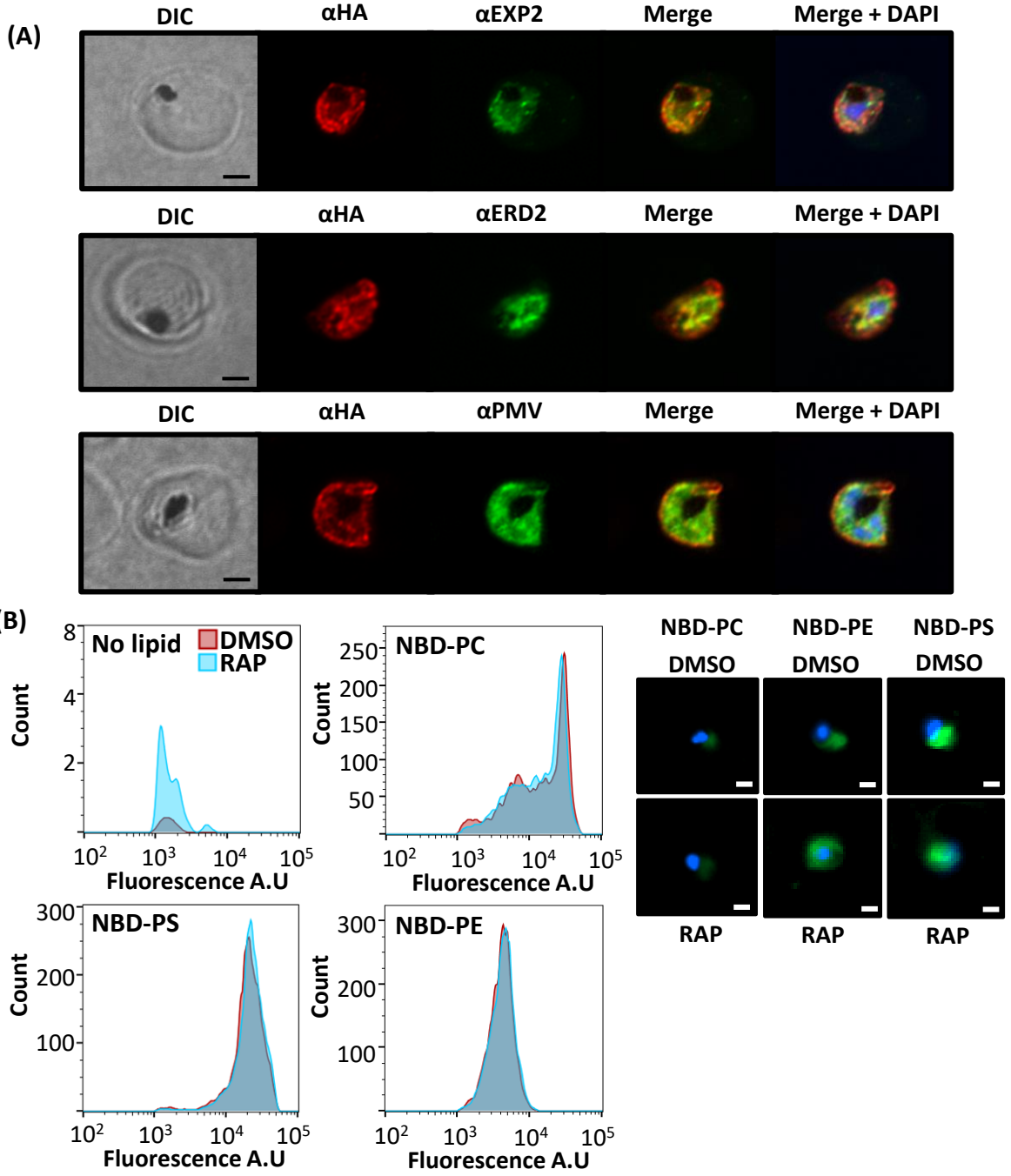
(A)
DIC
αHA
αEXP2
Merge
Merge + DAPI
DIC
αHA
αERD2
Merge
Merge + DAPI
DIC
αHA
αPMV
Merge
Merge + DAPI
(B)
No lipid
DMSO
RAP
Count
Fluorescence A.U
NBD-PC
NBD-PS
NBD-PE
NBD-PC
NBD-PE
NBD-PS
DMSO
DMSO
DMSO
RAP
RAP
RAP

Figure 6

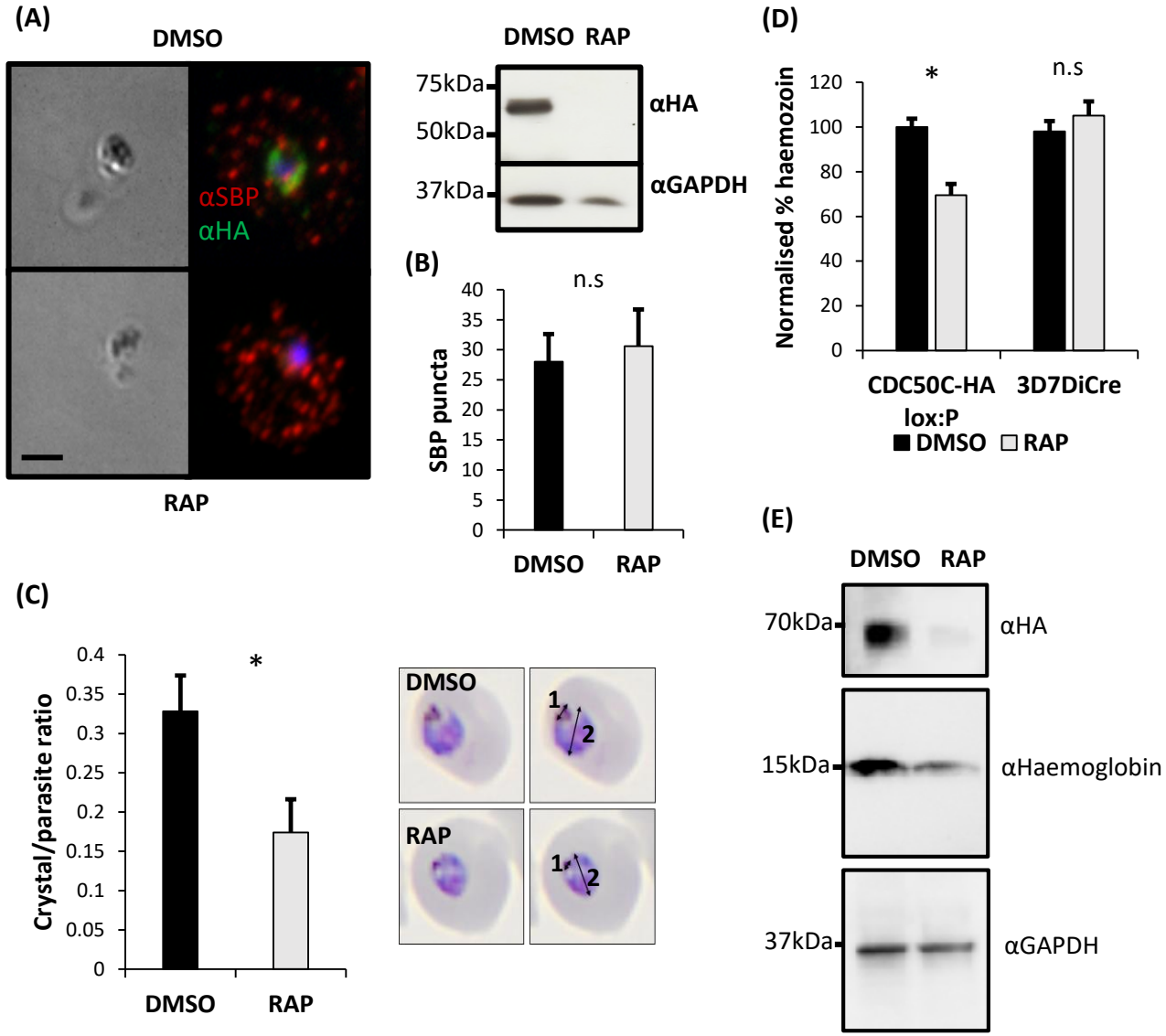
(A)
DMSO
αSBP
αHA
RAP
DMSO RAP
75kDa
50kDa
37kDa
αHA
αGAPDH
(B)
n.s
SBP puncta
40
35
30
25
20
15
10
5
0
DMSO
RAP
(C)
Crystal/parasite ratio
0.4
0.35
0.3
0.25
0.2
0.15
0.1
0.05
0
*
DMSO
RAP
DMSO
RAP
1
2
(D)
Normalised % haemozoin
120
100
80
60
40
20
0
*
n.s
CDC50C-HA lox:P
3D7DiCre
DMSO
RAP
(E)
DMSO RAP
70kDa
αHA
15kDa
αHaemoglobin
37kDa
αGAPDH